2800°C (8). Polyhedral nanoparticles (5 to 30 nm) made of concentric layers of closed graphene sheets with a nanoscale cavity in the center were produced at very high temperatures in arc plasma (9). They provide further evidence that nonplanar graphite crystals can exist. However, transformation of carbon polyhedra to onions under electron irradiation (9) suggested their instability. No other polyhedral carbon structures have been reported so far.

4. P. M. Ajayan, in *Carbon Nanotubes: Preparation and Properties*, T. W. Ebbesen, Ed. (CRC Press, Boca Raton, FL, 1997), pp. 111–138.
5. M. S. Dresselhaus, G. Dresselhaus, P. C. Eklund, *Science of Fullerenes and Carbon Nanotubes* (Academic Press, Burlington, MA, 1996).
6. S. Iijima, P. M. Ajayan, T. Ichihashi, *Phys. Rev. Lett.* **69**, 3100 (1992).
7. S. Iijima, *Mater. Res. Soc. Bull.* **19**, 43 (1994).
8. M. Endo, R. Saito, M. S. Dresselhaus, G. Dresselhaus, in *Carbon Nanotubes: Preparation and Properties*, T. W. Ebbesen, Ed. (CRC Press, Boca Raton, FL, 1997), pp. 35–110.
9. D. Ugarte, in *Carbon Nanotubes*, M. Endo, S. Iijima, M. S. Dresselhaus, Eds. (Pergamon, Oxford, 1996), pp. 163–167.
10. A. S. Fialkov, *Carbon, Intercalation Compounds and Composites on Its Base* (in Russian) (Aspect Press, Moscow, 1997).
11. K. Ray III and R. L. McCreery, *Anal. Chem.* **69**, 4680 (1997).
12. It was made from phenolic resin by carbonization at 2000°C in N_2 atmosphere at ~10 torr. The density of GC was 1.48 g/cm^3 with an open porosity of <1%. Its microstructure and properties are typical of other GCs. Total content of impurities (Si, Al, Ca, Ti, V, and Fe) is <100 parts per million. Hydrothermal treatment under 100 MPa at 750°C for 24 hours dissolves the GC matrix and allows for separation of stable crystalline structures contained in the pores for TEM and Raman spectroscopy studies. The composition and structure of GPC were examined with the use of Raman spectroscopy, which is the most powerful technique for identifying carbon allotropes (*14*), and electron microscopy. A Renishaw 2000 Raman microspectrometer with an Ar ion laser (514.5-nm excitation wavelength) was used. The TEMs used were a JEOL 3010 (300 kV) with the lattice resolution of 0.14 nm and JEOL 2010F (200 kV) with the lattice resolution of 0.1 nm. High resolutions in the scanning mode were achieved with the use of the JSM-6320 field emission scanning electron microscope (SEM). This microscope is also fitted with a Noran Voyager EDS system with a light element x-ray detector analyzer. Particles were deposited onto a Si wafer or polished aluminum sample holder for Raman and SEM studies, or onto a lacy carbon grid for TEM analysis. Raman and SEM studies were also conducted on fracture surfaces of GC pieces.
13. M. Liu and J. M. Cowley, *Ultramicroscopy* **53**, 333 (1994).
14. M. S. Dresselhaus, G. Dresselhaus, M. A. Pimenta, P. C. Eklund, in *Analytical Applications of Raman Spectroscopy*, M. Pelletier, Ed. (Blackwell Science, Oxford, 1999), pp. 367–434.
15. A. M. Rao, *et al.*, *Science* **275**, 187 (1997).
16. D. Ugarte, T. Stockli, J.-M. Bonard, A. Chatelain, W. A. DeHeer, in *The Science and Technology of Carbon Nanotubes*, K. Tanaka, T. Yamabe, K. Fukui, Eds. (Elsevier, Amsterdam, 1999), pp. 128–142.
17. H. Murayama and T. Maeda, *Nature* **345**, 791 (1990).
18. H. Hiura, T. W. Ebbesen, K. Tanigaki, H. Takahashi, *Chem. Phys. Lett.* **202**, 509 (1993).
19. R. D. Heidenreich, W. M. Hess, L. L. Ban, *J. Appl. Crystallogr.* **1**, 1 (1968).
20. E. J. W. Wittaker, *Acta Cryst.* **21**, 461 (1966).
21. Y. G. Gogotsi, V. P. Yaroshenko, F. Porz, *J. Mater. Sci. Lett.* **11**, 308 (1992).
22. T. W. Ebbesen, *Phys. Today* **June**, 26 (1996).
23. C. J. Brabec, A. Maiti, C. Roland, J. Bernholc, *Chem. Phys. Lett.* **236**, 150 (1995).
24. K. Tanaka *et al.*, in *The Science and Technology of Carbon Nanotubes*, K. Tanaka, T. Yamabe, K. Fukui, Eds. (Elsevier, Amsterdam, 1999), pp. 143–152.
25. S. Ihara and S. Itoh, in *Carbon Nanotubes*, M. Endo, S. Iijima, M. S. Dresselhaus, Eds. (Pergamon, Oxford, 1996), pp. 77–85.
26. E. Osawa, M. Yoshida, M. Fujita, *Mater. Res. Soc. Bull.* **19**, 33 (1994).
27. Supported in part by the Campus Research Board of the University of Illinois at Chicago and the Research Institute for Solvothermal Technology, Japan. The electron microscopes used in this work are operated by the Research Resources Center at the University of Illinois at Chicago. The JEM-2010F purchase was supported by the NSF.

3 July 2000; accepted 6 September 2000

The Fall, Recovery, Orbit, and Composition of the Tagish Lake Meteorite: A New Type of Carbonaceous Chondrite

Peter G. Brown,[1] Alan R. Hildebrand,[3] Michael E. Zolensky,[4] Monica Grady,[5] Robert N. Clayton,[6] Toshiko K. Mayeda,[6] Edward Tagliaferri,[7] Richard Spalding,[8] Neil D. MacRae,[9] Eric L. Hoffman,[10] David W. Mittlefehldt,[11] John F. Wacker,[12] J. Andrew Bird,[3] Margaret D. Campbell,[1] Robert Carpenter,[9] Heather Gingerich,[9] Michael Glatiotis,[3] Erika Greiner,[9] Michael J. Mazur,[3] Phil JA. McCausland,[9] Howard Plotkin,[2] Tina Rubak Mazur[3]

The preatmospheric mass of the Tagish Lake meteoroid was about 200,000 kilograms. Its calculated orbit indicates affinity to the Apollo asteroids with a semimajor axis in the middle of the asteroid belt, consistent with a linkage to low-albedo C, D, and P type asteroids. The mineralogy, oxygen isotope, and bulk chemical composition of recovered samples of the Tagish Lake meteorite are intermediate between CM and CI meteorites. These data suggest that the Tagish Lake meteorite may be one of the most primitive solar system materials yet studied.

Carbonaceous chondrites represent the most chemically unfractionated class of meteorites known (*1*). Much of our present understanding of early solar nebular chemistry, particularly organic chemistry, comes from the characterization of chondrites. One group of carbonaceous chondrites, the CI1's, have particularly primitive, solar-like compositions (*2, 3*), although all studied samples have been almost completely aqueously altered on the parent asteroid. The carbonaceous chondrites have been associated with the C types of asteroids (*4, 5*) primarily on the basis of their similar reflectance spectra, but no direct dynamical evidence linking these meteorites to specific asteroid populations has been previously available. Here, we present the preatmospheric orbit, mass, and initial compositional characterization of the Tagish Lake meteorite.

The fireball producing the Tagish Lake meteorite occurred on 18 January 2000 at 16:43 UT. This exceptionally bright fireball was witnessed in dawn twilight throughout the Yukon and Northwest territories, northern British Columbia, and parts of Alaska. The fireball was detected by infrared (IR) and optical sensors aboard U.S. Department of Defense satellites. Optical measurements placed the energy of the light flash at 1.1×10^{12} J. Bolides of H-chondrite composition have been found to have light-energy conversions of ~10% (*6*). A more realistic value for the present case is probably on the order of 5%, suggesting a total kinetic energy for the body of $\sim 2 \times 10^{13}$ J.

More than 70 eyewitnesses were interviewed to reconstruct the atmospheric trajec-

[1]Department of Physics and Astronomy, [2]Department of Philosophy, University of Western Ontario, London, Ontario N6A 3K7, Canada. [3]Department of Geology and Geophysics, University of Calgary, Calgary, Alberta T2N 1N4, Canada. [4]SN2, NASA Johnson Space Center, Houston, TX 77058, USA. [5]Department of Mineralogy, Natural History Museum, Cromwell Road, London SW7 5BD, UK. [6]Enrico Fermi Institute, Department of Chemistry, and Department of Geophysical Sciences, University of Chicago, 5640 South Ellis Avenue, Chicago, IL 60637, USA. [7]ET Space Systems, 5990 Worth Way, Camarillo, CA 93012, USA. [8]Sandia National Laboratories, Organization 5909, Mail Stop 0978, Post Office Box 5800, Albuquerque, NM 87185, USA. [9]Department of Earth Sciences, University of Western Ontario, London, Ontario N6A 5B7, Canada. [10]Activation Laboratories Ltd., 1336 Sandhill Drive, Ancaster, Ontario L9G 4V5, Canada. [11]Lockheed Martin SO, Houston, TX 77058, USA. [12]Pacific Northwest National Laboratory, Post Office Box 999, Richland, WA 99352, USA.

tory of the fireball. Additionally, a total of 24 still photos and five videos of the associated dust cloud were collected. Of these, a subset were timely (within 1 to 2 min of the event) and had sufficient foreground objects to permit angular measurements similar to those used to derive a trajectory for the Peekskill fireball (*7*). These have been incorporated into a solution for the path of the fireball created by the main mass of the meteoroid.

A synthesis of satellite optical data, features in the IR satellite record, and ground-based dust cloud photos indicate an estimated average velocity for the fireball of 15.5 ± 0.6 km s^{-1} from an azimuth of 331.5° ± 2.2° and an entry angle of 16.5° ± 1.2° from the horizontal. The most probable velocities are near the upper limit of the error range. Using the modeling techniques described in (*8*), we estimate the initial entry velocity to be 15.8 ± 0.6 km s^{-1}. This velocity, together with the total energy derived from the satellite data, suggests an initial entry mass for the meteoroid of 2×10^5 kg. Taking the estimated bulk density of the several hundred recovered samples of about 1500 kg m^{-3}, this corresponds to an initial body 4 to 6 m in diameter. Initial measurement of cosmogenic nuclides [see (*6*)] in Tagish Lake (Table 1) suggests that the parent meteoroid had a preatmospheric radius of between 2 and 4 m, consistent with the satellite data (*9*).

Orbital elements derived from the fireball entry velocity and path (Table 2) were compared to the four previous instrumentally determined meteorite orbits (Fig. 1). The calculated orbit for Tagish Lake is a typical Earth-crossing Apollo asteroid-type orbit with a semimajor axis in the middle of the asteroid belt. A dynamical linkage with outer-belt objects is possible [notably the C, D, and P type asteroids, which have spectra most similar to CM and CI chondrites (*10*)]. The uncertainties of the orbital elements are almost an order of magnitude larger than those of the four previously determined meteoroid orbits from which meteorites were recovered. The orbit also crosses much of the main belt at low inclination, which suggests that the source of the carbonaceous chondrites responsible for the xenoliths found in some meteorite breccias might be similar to the source of the Tagish Lake meteorite (*11, 12*).

The fireball ended in a series of detonations to the west and south of the town of Carcross, in the Yukon. Debris from these detonations crossed the Yukon–British Columbia border, and fragments landed on Taku Arm of Tagish Lake, at 59°42′N, 134°12′W (establishing the name of the meteorite). Jim Brook recovered the first specimens from the frozen lake surface on 25 January 2000. He continued collecting material on 26 January and was able to gather several dozen pieces in all, totaling ~0.85 kg. These fragments were collected from the surface of the frozen lake with ambient temperatures having remained subzero, and were placed in plastic bags without being handled by bare hands. All but one fragment has remained frozen since this initial collection. This rapid recovery minimized contamination and, combined with the frozen state of the meteorites, may permit characterization of the full range of volatile organics in a primitive chondrite.

Between 20 April and 8 May 2000, a dedicated field expedition located an additional 410 meteorite fragments on and below

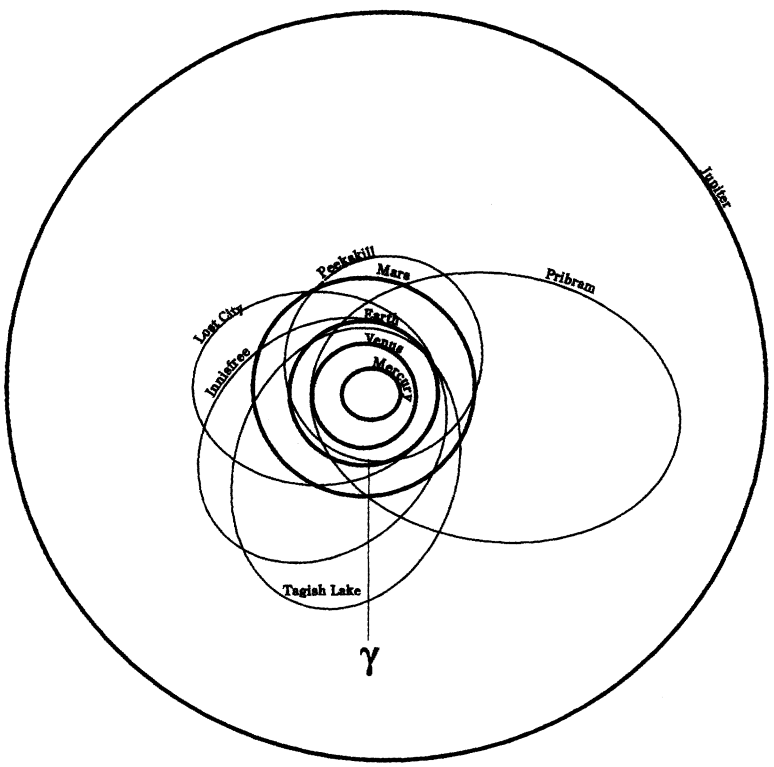

Fig. 1. The orbit of the Tagish Lake meteoroid, along with the four previous meteorite-producing fireballs with instrumentally determined orbits (Pribram, Lost City, Innisfree, and Peekskill). The symbol γ is the vernal equinox.

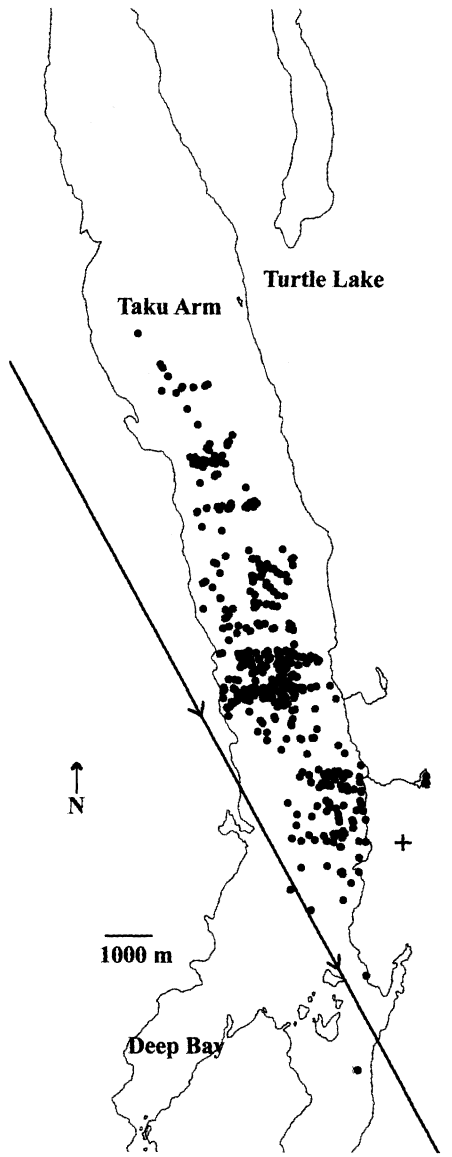

Fig. 2. Locations of meteorites recovered on the lake ice of Taku Arm (small dots). The line represents the direction of travel of the fireball. The observed fall ellipse is 16 km by 5 km, with the major axis oriented along an azimuth of ~150°. Fragments as large as 5 kg would have traveled 5 km further downrange. Gram-sized material from the first observed burst would have fallen a comparable distance uprange from the known distribution. The point marked "+" is latitude 59°42′N and longitude 134°11′W.

the ice surface of Taku Arm. All fragments collected in this way were variously degraded because of immersion in meltwater. A strewn field of minimum dimensions 16 km by 5 km extends from 59°39.5′N, 134°12′W to 59°48′N, 134°17′W (Fig. 2). Recovered masses ranged from ~2.3 kg in the south to subgram fragments in the extreme north of the fall ellipse (*13*). Aggregates and chips were recovered from most locales, although some individuals several hundred grams in mass were extracted intact. On the basis of recovery efficiency and fragment size distribution, we estimate that $>2 \times 10^3$ fragments larger than 1 g actually landed on the lake ice. More generally, we estimate a total of $>10^4$ fragments over the full fall ellipse, most of which is forested and mountainous terrain.

The classification of Tagish Lake is complex. One section of the Tagish Lake material collected on 25 January was examined using an electron microprobe (Fig. 3). Tagish Lake is a brecciated, matrix-supported mixture of olivine-rich aggregates, sparse chondrules (diameter <1 mm), probable altered calcium-aluminum-rich inclusions (CAIs) up to 2 mm in diameter, magnetite (mainly framboids and plaquettes), individual grains of olivine, Ca-Mg-Fe-Mn carbonates, and Fe-Ni sulfides including pyrrhotite.

Some chondrules and the majority of aggregates show evidence of aqueous alteration. The CAIs have the sinuous textures typical of CMs (*14*), but are almost completely altered to phyllosilicates, predominantly Mg-rich serpentine. In contrast, altered CAIs in CM chondrites usually consist of Fe-rich serpentine and diopside (*15*). Sulfides (in par-

Table 1. Cosmogenic radionuclide activities measured in four specimens of Tagish Lake.

Specimen mass (g)	Activity (decays min^{-1} kg^{-1})		
	Al^{26}	Na^{22}	Co^{60}
112	35 ± 2	50 ± 5	12 ± 2
9	35 ± 4	45 ± 7	41 ± 6
51	51 ± 3	86 ± 10	15 ± 2
96	43 ± 3	49 ± 5	41 ± 4

Table 2. Orbital parameters for the Tagish Lake meteorite. Angular elements are J2000.0.

a (semimajor axis)	2.1 ± 0.2 AU
e (eccentricity)	0.57 ± 0.05
q (perihelion distance)	0.891 ± 0.009 AU
ω (argument of perihelion)	222° ± 2°
Ω (longitude of ascending node)	297.900° ± 0.003°
i (inclination)	1.4° ± 0.9°
T (orbital period)	3.0 ± 0.4 years
DT (time since perihelion)	1072 ± 164 days
Q (aphelion distance)	3.3 ± 0.4 AU
V_{inf} (entry velocity)	15.8 ± 0.6 km/s

Table 3. Bulk element abundances for Tagish Lake. Abbreviations for methods: Prt-Gm, prompt gamma ray; LL/SL INAA, long-lived/short-lived INAA; TD-ICP, total digestion (HNO_3/$HCLO_4$/HF,HCl, 260°C) ICP-OES; WRA-ICP, whole rock analysis (lithium metaborate/tetraborate fusion) ICP-OES; F-ICPMS, lithium metaborate/tetraborate fusion ICP-MS; AQ-ICPMS, aqua regia digestion ICP-MS; C-IRA, combustion-IR analyzer; FA-INAA, nickel sulfide fire assay–INAA method (*25*). Values for Tagish Lake are the average of two analytical runs using two aliquots of starting material where available or based on separate analytical runs on the same solution where there was not enough material for two complete runs. Aliquot masses ranged from 0.057 to 0.358 g for the individual tests; details are available upon request to the authors. Where two techniques were used to measure the same element, both measures are given; deviations are the result of sample inhomogeneity. CI and CM carbonaceous chondrite bulk abundances (*26*) are given along with solar values for each element (*2*). The solar photosphere data were calculated by defining Si to be 10.64 wt % for direct comparison to CI values. Z, atomic number.

Z	Element	Unit	Method	CI	CM	Solar	Tagish Lake
1	H	wt %	Prt-Gm	2.02	1.4		1.5 ± 0.3
3	Li	ppm	TD-ICPMS	1.5	1.5	0.01071	2.5 ± 0.2
4	Be	ppm	TD-ICPMS	0.025	0.04	0.01359	0.052 ± 0.003
5	B	ppm	Prt-Gm	0.87	0.48	0.4594	0.8 ± 0.1
6	C	wt %	C-IRA	3.45	2.2		3.6 ± 0.2
11	Na	ppm	LL-INAA	5000	3900	5248	4450 ± 60
12	Mg	wt %	WRA-ICP	9.7	11.5	9.867	10.8 ± 0.5
13	Al	wt %	WRA-ICP	0.865	1.13	0.85	0.99 ± 0.03
14	Si	wt %	WRA-ICP	10.64	12.7	10.64	11.4 ± 0.4
15	P	ppm	TD-ICP	950	1030	931.7	927 ± 50
16	S	wt %	C-IRA	5.41	2.7	5.553	3.8 ± 0.2
17	Cl	ppm	SL-INAA	700	430	1197	560 ± 90
19	K	ppm	TD-ICP	550	370	550.2	650 ± 50
20	Ca	wt %	WRA-ICP	0.926	1.29	0.9803	0.99 ± 0.09
21	Sc	ppm	LL-INAA	5.9	8.2	6.043	7.2 ± 0.3
22	Ti	ppm	WRA-ICP	440	550	499.4	520 ± 56
23	V	ppm	F-ICPMS	55	75	54.38	57 ± 3
23	V	ppm	SL-INAA	55	75	54.38	51 ± 1
24	Cr	ppm	LL-INAA	2650	3050	2596	2840 ± 150
25	Mn	ppm	WRA-ICP	1940	1650	1440	1450 ± 150
25	Mn	ppm	SL-INAA	1940	1650	1440	1530 ± 77
26	Fe	wt %	LL-INAA	18.2	21.3	27.89	19.3 ± 0.9
27	Co	ppm	LL-INAA	505	560	523.3	517 ± 9
28	Ni	wt %	LL-INAA	1.1	1.23	1.114	1.16 ± 0.08
29	Cu	ppm	TD-ICP	125	130	110.0	116 ± 5
30	Zn	ppm	TD-ICP	315	180	277.9	253 ± 9
31	Ga	ppm	F-ICPMS	9.8	7.6	5.646	8.4 ± 0.3
32	Ge	ppm	F-ICPMS	33	26		30 ± 2
33	As	ppm	LL-INAA	1.85	1.8		1.74 ± 0.06
34	Se	ppm	LL-INAA	21	12		14.3 ± 0.4
35	Br	ppm	LL-INAA	3.5	3.0		2.8 ± 0.2
37	Rb	ppm	F-ICPMS	2.3	1.6	3.633	2.0 ± 0.2
38	Sr	ppm	F-ICPMS	7.3	10	7.43	9.4 ± 0.5
39	Y	ppm	F-ICPMS	1.56	2.0	1.65	1.7 ± 0.1
40	Zr	ppm	F-ICPMS	3.9	7.0	3.877	6.0 ± 1.3
41	Nb	ppm	F-ICPMS	0.25	0.4	0.2609	0.31 ± 0.15
42	Mo	ppm	AQ-ICPMS	0.92	1.4	0.8520	1.13 ± 0.09
44	Ru	ppm	FA-INAA	0.71	0.87	0.7467	1.08 ± 0.09
45	Rh	ppm	FA-INAA	0.14	0.16		0.25 ± 0.02
46	Pd	ppm	FA-INAA	0.56	0.63	0.5564	0.98 ± 0.09
47	Ag	ppm	AQ-ICPMS	0.2	0.16	0.1003	0.21 ± 0.07
48	Cd	ppm	AQ-ICPMS	0.69	0.42	0.8693	0.82 ± 0.16
49	In	ppm	F-ICPMS	0.08	0.05	0.5602	0.060 ± 0.007
49	In	ppm	AQ-ICPMS	0.08	0.05	0.5602	0.075 ± 0.005
50	Sn	ppm	F-ICPMS	1.7	0.79	1.267	0.92 ± 0.09
51	Sb	ppm	LL-INAA	0.135	0.13	0.13	0.17 ± 0.03
52	Te	ppm	AQ-ICPMS	2.3	1.3		1.5 ± 0.3
53	I	ppm	SL-INAA	0.43	0.27		<0.2
55	Cs	ppm	F-ICPMS	0.19	0.11		0.146 ± 0.006
56	Ba	ppm	F-ICPMS	2.35	3.1	1.977	3.6 ± 1.2
56	Ba	ppm	TD-ICPMS	2.35	3.1	1.977	7.4 ± 0.8
57	La	ppm	F-ICPMS	0.235	0.32	0.2462	0.31 ± 0.02
57	La	ppm	LL-INAA	0.235	0.32	0.2462	0.33 ± 0.03
58	Ce	ppm	F-ICPMS	0.62	0.94	0.5307	0.81 ± 0.06
59	Pr	ppm	F-ICPMS	0.094	0.137	0.07715	0.111 ± 0.007
60	Nd	ppm	F-ICPMS	0.46	0.626	0.4868	0.58 ± 0.03
62	Sm	ppm	F-ICPMS	0.15	0.204	0.1606	0.19 ± 0.02
62	Sm	ppm	LL-INAA	0.15	0.204	0.1606	0.20 ± 0.02
63	Eu	ppm	F-ICPMS	0.057	0.078	0.05251	0.072 ± 0.004
64	Gd	ppm	F-ICPMS	0.2	0.29	0.2213	0.24 ± 0.02

Table 3 *Continued.*

Z	Element	Unit	Method	CI	CM	Solar	Tagish Lake
65	Tb	ppm	F-ICPMS	0.037	0.051	0.01347	0.049 ± 0.005
66	Dy	ppm	F-ICPMS	0.25	0.332	0.2184	0.30 ± 0.04
67	Ho	ppm	F-ICPMS	0.056	0.077	0.03204	0.064 ± 0.006
68	Er	ppm	F-ICPMS	0.16	0.221	0.1520	0.20 ± 0.02
69	Tm	ppm	F-ICPMS	0.025	0.035	0.01803	0.032 ± 0.002
70	Yb	ppm	F-ICPMS	0.16	0.215	0.2220	0.203 ± 0.009
70	Yb	ppm	LL-INAA	0.16	0.215	0.2220	0.21 ± 0.02
71	Lu	ppm	F-ICPMS	0.025	0.033	0.1075	0.032 ± 0.001
71	Lu	ppm	LL-INAA	0.025	0.033	0.1075	0.034 ± 0.006
72	Hf	ppm	F-ICPMS	0.105	0.18	0.1446	0.18 ± 0.02
73	Ta	ppm	F-ICPMS	0.014	0.019		0.022 ± 0.006
75	Re	ppm	AQ-ICPMS	0.038	0.050		0.056 ± 0.004
76	Os	ppb	FA-INAA	490	670	572.2	460 ± 18
77	Ir	ppb	FA-INAA	465	580	459.4	547 ± 10
78	Pt	ppm	FA-INAA	1.0	1.1		1.22 ± 0.05
79	Au	ppm	LL-INAA	0.145	0.150	0.2152	0.19 ± 0.03
81	Tl	ppm	TD-ICPMS	0.142	0.092	0.1733	0.090 ± 0.004
82	Pb	ppm	AQ-ICPMS	2.50	1.6	1.566	2.9 ± 0.8
83	Bi	ppm	AQ-ICPMS	0.11	0.071		0.09 ± 0.02
90	Th	ppm	F-ICPMS	0.029	0.041	0.03264	0.040 ± 0.008
92	U	ppm	F-ICPMS	0.008	0.012	0.008608	0.008 ± 0.004

ticular the coarse-grained sulfides present in CIs and all of the metamorphosed carbonaceous chondrites) (*16*) are less abundant than in most CM or CI chondrites, and magnetite is far more abundant than in most CMs (*14*). In many places, magnetite has partially or completely replaced sulfides. Carbonates in Tagish Lake vary in composition from calcite ($CaCO_3$) to siderite ($FeCO_3$) and magnesite ($MgCO_3$). These end-member Mg- and Fe-rich compositions are not found in any other carbonaceous chondrites (*15*). Some carbonates have Mn contents up to 1 weight percent (wt %). Olivine has the compositional range Fa_{0-29} [percent mean deviation (PMD) = 2%] with a peak at Fa_1; pyroxene is Fs_{1-7} (PMD = 2%), with a peak at Fs_2. The meteorite shock stage is S1, which is typical for carbonaceous chondrites. The microprobe data indicate that the matrix consists mainly of phyllosilicates, probably intergrown serpentine and saponite.

Oxygen isotope measurements were made on two 5-mg portions of uncontaminated Tagish Lake, one yielding $\delta^{18}O = +19.0$ per mil (‰), $\delta^{17}O = +9.2$‰ and the other yielding $\delta^{18}O = +18.0$‰, $\delta^{17}O = +8.3$‰ (*17*). This rather large difference may reflect sample heterogeneity. The isotopic compositions (Fig. 4) are far removed from the field of CM chondrites and are more similar to those of CI chondrites and of a group of metamorphosed carbonaceous chondrites (such as Belgica 7904, Yamato 82162, and Yamato 86720) (*1*). If the data on Tagish Lake are interpreted in terms of the model of exchange of minerals with liquid water on a parent body (*1*), the oxygen isotopic data suggest a higher water/rock ratio than the CM group, and a lower temperature of aqueous alteration (near 0°C) than the CI group.

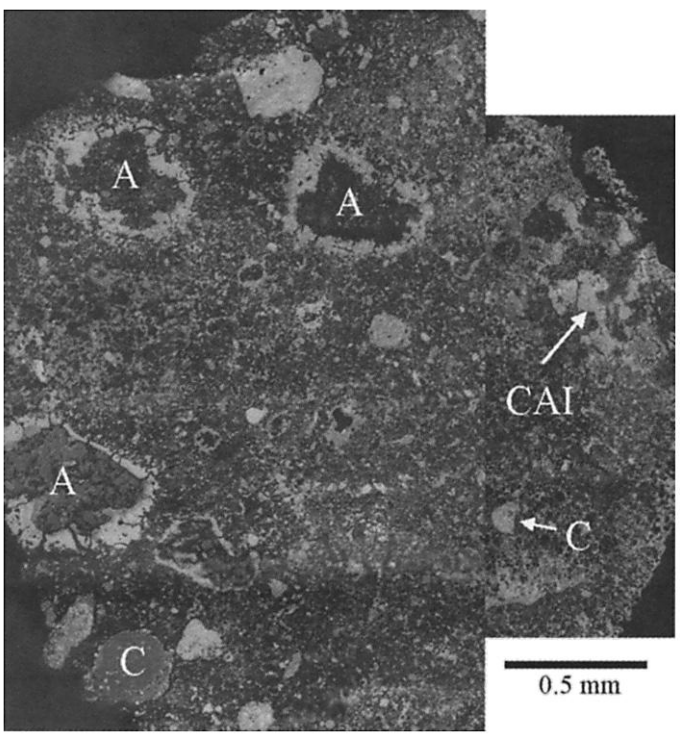

Fig. 3. Backscattered electron image of two polished chips of Tagish Lake. A few chondrules (C), olivine aggregates (A), and one CAI can be seen in the matrix-dominated material. The majority of the opaques (bright-appearing phases) are magnetite.

Carbon concentration and isotopic composition were determined by high-resolution stepped-combustion mass spectrometry of a 1.0174-mg chip (*18*). The total carbon yield was 5.4 wt %, with summed $\delta^{13}C \sim +24.3$‰. The yield is higher than typical for CI and CM chondrites (*19*), possibly reflecting local sample heterogeneity given the small mass used. The carbon isotopic composition is also unusually high for either CI or CM chondrites [generally –15 to 0‰ (*19*)], a reflection of the abundant ^{13}C-rich carbonates in Tagish Lake. There are several carbon-bearing components present. Maxima in the yield histogram at 500°C ($\delta^{13}C \sim +43$‰) and 600°C ($\delta^{13}C \sim +56$‰) are inferred to correspond to the decrepitation of Fe-Mg carbonate and Ca carbonate, respectively (Fig. 5). Around 3.7 wt % carbon derives from carbonates (mainly Fe-Mg–rich), a much higher proportion than is usual for either CI or CM chondrites, where 0.2 to 0.5 wt % carbon typically occurs as carbonate; the carbon isotopic composition of the carbonate, however, is within the range of values for CI and CM chondrites [+20 to +70‰ (*20*)]. The remaining carbon is mostly from organic species that combust below ~500°C. The $\delta^{13}C$ of the organics varies from −10 to −1‰, a range similar to that observed for organic species in CI and CM meteorites (*21*).

In addition to the major carbon-bearing phases, large excursions in isotopic composition indicate the presence of interstellar grains within Tagish Lake. We clearly detect nanodiamonds (combusting at 525° to 550°C, depleted in ^{13}C) and silicon carbide (combusting above 1000°C, enriched in ^{13}C) in Tagish Lake, and the presence of both components is matched by similar excursions in $\delta^{15}N$ during nitrogen release.

Results of the bulk composition determinations (Table 3) (*22*) indicate that the refractory lithophile element (Zr-Sr) abundances are more similar to those of CM chondrites, whereas the moderately volatile and volatile lithophile element (Mn-Br) abundances are between those of CM and CI chondrites. The refractory siderophile element (Re-Pd) abundances are like those of both CI and CM chondrites, whereas the

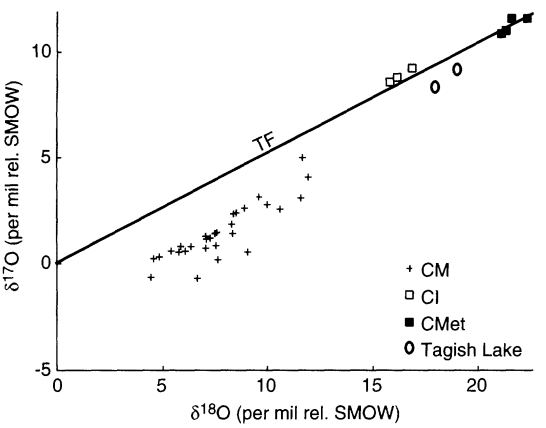

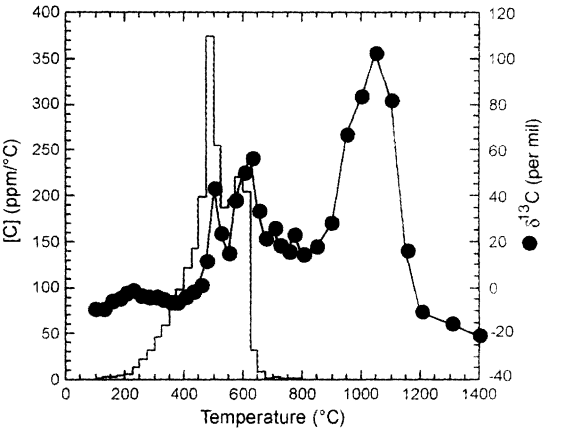

Fig. 4 (left). Three-isotope plot for CI, CM, and metamorphosed (CMet) carbonaceous chondrites [data from (*1*)]. Tagish Lake compositions (ovals) are unlike all previously analyzed groups but are closest to the CI group. **Fig. 5 (right).** Carbon release as a function of heating temperature for Tagish Lake, with corresponding $\delta^{13}C$ values. The vertical bars show the concentration of carbon released at each temperature increment (scale on the left-side ordinate); the solid dots represent the per mil difference in the isotope ratios of ^{13}C to ^{12}C relative to the C standard (scale on the right-side ordinate) for the carbon released at each temperature.

moderately volatile and volatile siderophile element (Au-Tl) and volatile chalcophile element (Zn-Cd) abundances are generally between those of CI and CM chondrites. The bulk composition alone does not allow a definitive classification to be made. The refractory element abundances are compatible with assignment to the CM group, but the moderately volatile and volatile element abundances indicate that such an assignment is not warranted.

On the basis of these data, we suggest that Tagish Lake is more primitive than type 1 CI chondrites (*23*). Tagish Lake may therefore represent samples of the precursor lithology to CI1 with a possible relation to metamorphosed carbonaceous chondrites such as Yamato 82162 (*24*). We tentatively conclude that Tagish Lake is a new type of carbonaceous chondrite. We note, however, that there are no examples of CI2 chondrites, and we do not rule out the possibility that Tagish Lake's unusual chemical and isotopic characteristics are due to its being a less altered CI chondrite. As a result, the bulk composition of Tagish Lake may serve as a more useful model of the solar abundances of the elements (*2*).

References and Notes

1. R. N. Clayton and T. K. Mayeda, *Geochim. Cosmochim. Acta* **63**, 2089 (1999).
2. E. Anders and N. Grevesse, *Geochim. Cosmochim. Acta* **53**, 197 (1989).
3. For carbonaceous chondrites, M and I (group) refer to differences in bulk composition (including O isotopes); 1, 2, and 3 (petrologic grade) refer to degree of aqueous alteration, where 3 is most pristine and 1 is most altered. It is possible that the groups derive from different asteroids while the different petrologic grades originate from different regions of each asteroid.
4. T. Hiroi, M. E. Zolensky, C. M. Pieters, M. E. Lipschutz, *Meteor. Planet. Sci.* **31**, 321 (1996).
5. Asteroids are classified according to the shape of their reflectance spectra and albedo. The C asteroids have spectra similar to the more primitive carbonaceous chondrites and (from the shape of their spectra) are believed to be rich in carbon, clays, and organics. The D and P asteroids show spectral signatures suggestive of low-temperature compounds such as complex organics, water, and volatiles. D and P asteroids tend to be darker than C asteroids, are most numerous in the outer part of the asteroid belt, and have no known meteorite analogs.
6. P. Brown *et al.*, *Meteor. Planet. Sci.* **31**, 502 (1996).
7. P. Brown *et al.*, *Nature* **367**, 624 (1994).
8. Z. Ceplecha *et al.*, *Adv. Space Res.* **84**, 327 (1998).
9. For most meteorite falls, increasing activities of spallation (e.g., ^{22}Na, ^{26}Al) and neutron-activated (e.g., ^{60}Co) cosmogenic nuclides correlate with increasing prefall meteoroid size. However, spallation and activation products' concentrations begin to decline at radii of ~50 cm [N. Bhandari *et al.*, *Geochim. Cosmochim. Acta* **57**, 23611 (1993); I. Leya *et al.*, *Meteor. Planet. Sci.* **259**, 35 (2000)] and ~80 cm [M. S. Spergel *et al.*, *Lunar Planet. Sci.* **XVI**, 756 (1986)], respectively. The low density of the Tagish Lake meteorites relative to the modeled and measured densities of ordinary chondrites in previous studies will result in an approximate doubling of the corresponding radii. Measured ^{22}Na and ^{26}Al activities indicate derivation of the surveyed meteorite fragments from depths of about 1 to 2 m in an object of >2 m radius. The measured activities are higher than that expected in the case of 2π irradiation geometry, indicating that the meteoroid was not larger than ~4 m radius. For activated nuclides, the effect of declining activities toward the meteoroid's center will be accentuated by the Tagish Lake meteoroid's substantial light element (H, C) content, resulting in the neutron flux peaking closer to the surface and decreasing more rapidly with depth than in ordinary chondrites. Thus, if the Tagish Lake meteoroid had a radius substantially larger than 2 m, high ^{60}Co activities will not be present (e.g., all ^{60}Co abundances will be below the 51 to 79 decays min^{-1} kg^{-1} measured in the Murchison CM2 chondrite, which was presumably derived from a smaller meteoroid) [P. J. Cressy, *J. Geophys. Res.* **76**, 4905 (1972); J. C. Evans *et al.*, *J. Geophys. Res.* **87**, 5577 (1982)].
10. J. C. Gradie, C. R. Chapman, E. F. Tedesco, in *Asteroids II*, R. P. Binzel, T. Gehrels, M. S. Matthews, Eds. (Univ. of Arizona Press, Tucson, AZ, 1989), pp. 316–335.
11. M. E. Lipschutz, M. J. Gaffey, P. Pellas, in *Asteroids II*, R. P. Binzel, T. Gehrels, M. S. Matthews, Eds. (Univ. of Arizona Press, Tucson, AZ, 1989), pp. 740–777.
12. M. E. Zolensky *et al.*, *Meteor. Planet. Sci.* **31**, 518 (1996).
13. The distribution of fragments on the ground occurs over an ellipse-shaped region, with the largest meteorites farthest along the major axis of this fall ellipse.
14. M. E. Zolensky *et al.*, *Geochim. Cosmochim. Acta* **57**, 3123 (1993).
15. M. E. Zolensky *et al.*, *Geochim. Cosmochim. Acta* **61**, 5099 (1997).
16. M. E. Lipschutz *et al.*, *Antarct. Meteorite Res.* **12**, 57 (1999).
17. Mass spectrometric uncertainties are about 0.1 per mil (2σ) for both $\delta^{18}O$ and $\delta^{17}O$. In addition, mass-dependent fractionation effects on the order of 1 per mil may result from partial dehydration of phyllosilicates during evacuation and degassing before fluorination. See R. N. Clayton and T. K. Mayeda [*Geochim. Cosmochim. Acta* **67**, 151 (1984)] for an illustration of this effect in Orgueil.
18. Mass spectrometry was performed using a high-sensitivity static vacuum system at Open University. With this technique, stepped heating produces peaks in the quantity of gaseous carbon released as the combustion temperature for each carbon phase is reached. For details of the techniques used, see S. J. Prosser, I. P. Wright, C. T. Pillinger, *Chem. Geol.* **83**, 71 (1990); P. D. Yates, I. P. Wright, C. T. Pillinger, *Chem. Geol.* **101**, 81 (1992). The samples (wrapped in platinum foil) were heated in the presence of pure oxygen gas in increments from room temperature to 1400°C. Combustion products were converted to CO_2 using a combination of heated Cu/CuO and Pt. Other elements such as sulfur and hydrogen also give oxidation products, so the resultant gases were separated cryogenically; isotopic compositions were determined on pure CO_2 using a triple-collector noble gas–type mass spectrometer operated in static mode. Carbon yields were measured on a capacitance manometer to ±0.2 ng, and $\delta^{13}C$ was measured to ±0.5 per mil on sample sizes down to ~5 ng.
19. J. F. Kerridge, *Geochim. Cosmochim. Acta* **49**, 1707 (1985); R. N. Clayton and T. K. Mayeda, *Annu. Rev. Earth Planet. Sci.* **21**, 115 (1993).
20. M. M. Grady *et al.*, *Geochim. Cosmochim. Acta* **52**, 2855 (1988).
21. J. R. Cronin and S. Chang, in *The Chemistry of Life's Origins*, J. M. Greenberg, C. X. Mendoza-Gomez, V. Pirronello, Eds. (Kluwer, Dordrecht, Netherlands, 1993), pp. 209–258.
22. Bulk measurements were made using prompt gamma, instrumental neutron activation analysis (INAA), inductively coupled plasma (ICP), ICP mass spectrometry (ICP-MS), and combustion-IR analyses. Bulk elemental values for the Tagish Lake material were analyzed together with two aliquots of the Tagish Lake degraded material, two aliquots of the Allende meteorite control, and a variety of international certified standard reference materials of similar mass. The samples and standards were analyzed for boron and hydrogen by prompt gamma analysis using the McMaster University Nuclear Reactor Prompt Gamma Facility. The samples were irradiated at a flux of 7×10^{12} neutrons cm^{-2} s^{-1} in the McMaster Nuclear Reactor computer-controlled rabbit irradiation site for both thermal (60 s) and epithermal (5 min) irradiations. Samples were counted on a high-purity germanium counting system (resolution of 2.0 KeV for the 1332-KeV Co^{60} photopeak) for 100 s after a decay of 7 min. Samples were recounted for 300 s after a decay of 30 and 75 min. Samples, standards and blanks, and flux monitors were then combined in a batch and were reirradiated for 3 hours in the RIFLS irradiation facility of the McMaster Nuclear Reactor.

After a decay of 4 days, 5 days, 7 days, and 8 days, samples were remeasured on a high-resolution Ge detector system (resolution of 1.61 KeV for the Co^{60}, 1332 KeV photopeak). The same sample material used above was then fused with a combination of lithium metaborate/tetraborate and lithium carbonate in high-purity graphite crucibles covered with graphite lids in an induction furnace. The molten mixture was transferred to a 5% (by volume) nitric acid (with Cd internal standard) solution. The molten bead immediately shattered and was shaken until totally dissolved (~15 min). Masses of 0.05-g aliquots in duplicate were analyzed by combustion-IR techniques using an ELTRA simultaneous carbon/sulfur analyzer, Model 800. A sequence of 0.1-g aliquots were digested with aqua regia at 90°C for 2 hours. Finally, a 0.1-g aliquot was subjected to an 18-hour ramped digestion in Teflon test tubes using hydrochloric, nitric, perchloric, and hydrofluoric acids. Samples were analyzed by ICP–optical emission spectrometry (OES) on a Perkin-Elmer OPTIMA 3000 ICP-OES and a Perkin-Elmer SCIEX ELAN 6000 and 6100. We noted systematically higher values in all cases for degraded (immersed in lake water) as compared to pristine meteorite abundances, except for H, Na, and Cl, which were much lower in the degraded specimens than in the pristine material. The H anomaly is probably due to excess removal of indigenous water in the degraded sample; it is very common for CI chondrites to contain large amounts (in excess of 10 wt %) of primordial water [L. Baker *et al.*, *Lunar Planet. Sci.* **XXIX**, 1740 (1998)]. The large difference in Na and Cl between pristine and water-soaked samples might be interpreted as removal of water-soluble halite from Tagish Lake. Halite has been previously reported in H chondrites [M. E. Zolensky *et al.*, *Science* **285**, 1377 (1999)]. This indirect indication of halite in a carbonaceous chondrite would therefore be unsurprising.

23. H. Y. McSween, *Rev. Geophys. Space Phys.* **17**, 1059 (1979).
24. K. Tomeoka, H. Kojima, K. Yanai, *Proc. NIPR Symp. Antarct. Meteorites* **2**, 36 (1989).
25. E. L. Hoffman *et al.*, *Anal. Chem. Acta* **102**, 157 (1978).
26. K. Lodders and B. Fegley, *The Planetary Scientist's Companion* (Oxford Univ. Press, Oxford, 1998), pp. 314–316.

27. We thank J. Brook, D. Stangel, and M. Brook for assistance in meteorite recovery work; R. Halliday, M. Jasek, E. Magnuson, and C. R. Roots for assistance in interviewing and locating the many eyewitnesses in the Yukon and British Columbia, who also provided still photos and video of the fireball dust cloud; the Royal Canadian Mounted Police for conducting experiments in meteorite recovery with one of its tracking dogs; C. Pillinger and A. B. Verchovsky for use of and assistance with analytical facilities for the carbon systematics; F. Saunders, manager of the reactor, for free use of all irradiation facilities; H. Y. McSween, M. E. Lipschutz, and H. W. Nesbitt for helpful reviews of an earlier version of this manuscript; and two anonymous referees. Analyses by prompt gamma ray and short-lived INAA were provided by A. Pidruczny of the McMaster Nuclear Reactor. Carbon and sulfur analyses were provided by Actlabs-Skyline, Tucson, AZ; INAA, ICP, and ICP-MS facilities were provided at no cost by Activation Laboratories Ltd., Ancaster, Ontario. The nickel sulfide fire assay was done by C.-T. Wu, University of Western Ontario. The fireball trajectory analysis software was developed by J. Borovicka and Z. Ceplecha. Field data collection was supported by NASA–Johnson Space Center, Sandia National Laboratories, the University of Calgary, and the University of Western Ontario. Supported by grants from the Particle Physics and Astronomy Research Council (C. T. Pillinger and M.G.) and NSF grant EAR9815338 (R.C.).

7 August 2000; accepted 8 September 2000

The Last Glacial–Holocene Transition in Southern Chile

K. D. Bennett,[1]* S. G. Haberle,[2] S. H. Lumley[3]

Warming at the last glacial termination in the North Atlantic region was interrupted by a period of renewed glacial activity during the Younger Dryas chronozone (YDC). The underlying mechanism of this cooling remains elusive, but hypotheses turn on whether it was a global or a North Atlantic phenomenon. Chronological, sedimentological, and palaeoecological records from sediments of small lakes in oceanic southern Chile demonstrate that there was no YDC cooling in southern Chile. It is therefore likely that there was little or no cooling in southern Pacific surface waters and hence that YDC cooling in the North Atlantic was a regional, rather than global, phenomenon.

The YDC [13 to 11.2 thousand years before the present (ky BP) (*1*)] in northern Europe was a period of renewed glacial activity after the decline of the main last glacial ice mass. The temperature changes of the period are seen most strongly in oceanic western Europe, and their amplitude decreases eastward into the continental interior (*2*). A cooling during this period has also been recognized in eastern North America (*3*) and correlated with event stratigraphy from the Greenland Ice Core Project (GRIP) (*4*). Here we present chronological, sedimentological, and pollen data from the sediments of small lakes in oceanic southern Chile (44° to 47°S), chosen to be as similar as possible in character and location to sites in the North Atlantic region that demonstrate strong temperature changes during the YDC. We show that there was no cooling and that the YDC was a period of continuing forest development and increasing diversity. The climate of this region is dominated by air masses from the Pacific and the north-flowing Humboldt Current, which originates as an eastward flow across the southern Pacific (*5*). If there was no cooling during the YDC in southern Chile, it is unlikely that there can have been any cooling in southern Pacific surface waters; hence, the cooling during the YDC in the North Atlantic was a regional, rather than global, phenomenon.

In temperate areas of moderate and high precipitation, small lakes remain full to their outlets, retaining a constant deep-water anoxic environment at their base. The sediments in such lakes consist largely of the remains of planktonic algae, atmospheric dust, and material washed from surrounding slopes. Such sediments may thus be highly stable as sedimentary environments, preserving materials indicative of conditions in aquatic, terrestrial, and atmospheric environments. We sampled the sediments of a series of lakes on the Taitao peninsula and an islands of the Chonos archipelago in southern Chile (Fig. 1), choosing lakes that were located in rock basins, had no inflowing streams, and were still moderately deep (2 to 5 m) for their size (100 m diameter). Such sites should be the most sensitive to any temperature changes of the period, as in western Europe (*6–8*). Cores were collected with a Livingstone piston corer. On return to the laboratory, they were analyzed immediately for physical properties and sampled for radiocarbon dating [bulk and accelerator mass spectrometry (AMS)] and the presence of tephras to provide a chronology, and the pollen content was assessed at intervals of 100 to 150 years or less.

All cores from these lakes showed similar simple stratigraphies. Basal sediments were always gray silty clays, succeeded upward by brown algal gyttja (Fig. 2). Magnetic susceptibility measurements confirmed visual inspection, showing no evidence along the sequences for changes (such as increases in eroded inorganic material) that might indicate a period of cooling. Radiocarbon age determinations (*9, 10*) allowed us to pinpoint sediments of the YDC in each core, and confirmed that there were no sedimentary changes during this period. Detailed tephrochronological analyses of these and other cores from the region (*10*), which include tephras within the Last Glacial, confirm and support the radiocarbon chronology (*11*).

Forest development, determined from the pollen analyses (Figs. 3 and 4) (*12*), began about 14 ky BP with the arrival and increase of southern beech *Nothofagus*, probably *Nothofagus betuloides* (*13*). The landscape became completely forested as other trees followed (Fig. 3). The sequence of trees is broadly (*Tepualia* is the only exception) in

[1]Quaternary Geology, Department of Earth Sciences, Uppsala University, Villavägen 16, S-752 36 Uppsala, Sweden. [2]Department of Geography and Environmental Science, Monash University, Clayton, Victoria 3168, Australia. [3]53 Cavendish Road, Cambridge CB1 3EA, UK.

*To whom correspondence should be addressed. E-mail: Keith.Bennett@geo.uu.se